Fundamentals of Inertial Focusing in High Aspect Ratio Curved Microfluidics

Javier Cruz (javier.cruz@angstrom.uu.se)
Uppsala University
Klas Hjort
Uppsala University

Research Article

Keywords: Microfluidics, High Aspect Ration Curved (HARC), high-quality position, inertial microfluidics

Posted Date: December 11th, 2020

DOI: https://doi.org/10.21203/rs.3.rs-123615/v1

Version of Record: A version of this preprint was published at Scientific Reports on March 19th, 2021. See the published version at https://doi.org/10.1038/s41598-021-85910-2.

ARTICLE

Fundamentals of Inertial Focusing in High Aspect Ratio Curved Microfluidics

MST Division

Uppsala University

December 2020

Javier Cruz*[a] and Klas Hjort*[a]

Microfluidics exploiting the phenomenon of inertial focusing have attracted much attention in the last decade, as they provide the means to facilitate the detection and analysis of rare particles of interest in complex fluids such as blood and natural water. Although many interesting applications have been demonstrated, the systems remain difficult to engineer. A recently presented line of the technology, inertial focusing in High Aspect Ration Curved (HARC) microfluidics, has the potential to change this and make the benefits of inertial focusing more accessible to the community. In this paper, with experimental evidence and fluid simulations, we provide the two necessary equations to design the systems and successfully focus the desired targets in a single, stable, and high-quality position. Last, the experiments revealed an interesting scaling law of the lift force, which we believe provides a valuable insight into the phenomenon of inertial microfluidics.

Introduction

Inertial focusing is a phenomenon that enables focusing of initially randomly distributed particles in a fluid into well-defined positions within the microfluidic channels, thereby facilitating the detection, isolation and analysis of rare targets of interest in complex fluid samples like blood, for instance. The technology has attracted much attention over the last decade thanks to its attributes; it allows for high through-put focusing, concentration and separation of particles with high resolution, it does not require labelling of the targets, it works for neutrally buoyant particles, and the operation of the systems is relatively simple (the sample simply has to pass through the microchannel at a controlled flow rate)[1–3]. With such a promising performance, the technology has grown rapidly.

The phenomenon has been physically and analytically described[4–9] since it was first observed by Segré & Silberberg in 1961[10]. Migration of particles occurs in microfluidic systems where inertia is not negligible, and it is attributed to a lift force (F_L) induced by the interaction of the fluid with the particles and the walls of the microchannels, which is often complemented by the drag of a secondary flow (F_D) to reduce the number of focus positions and tune their location. Multiple successful applications of the phenomenon have been presented, such as isolation and extraction of circulating tumour cells (CTC) from blood samples[11,12] and focusing, separation and concentration of pathogenic bacteria from water samples[13,14].

A notable limitation is the rapid increase in the pressure needed to run the systems when targeting submicron particles[13]. Although robust silicon-glass systems have been shown to withstand up to 200 bar and allow for focusing particles down to 0.5 μm[14],

[a] *Division of Microsystems Technology, Uppsala University, Ångström Laboratory, Uppsala, Sweden.*

*Corresponding authors:
Klas Hjort klas.hjort@angstrom.uu.se
Javier Cruz javier.cruz@angstrom.uu.se

Electronic Supplementary Information (ESI) available

smaller particles of interest such as viruses or exosomes still remain a challenge for the technology. Another major limitation for the technology is the fact that the position of the focused particles (focus position) generally depends on multiple variables. In fact, the focus position generally shifts in tortuous ways as a function of all variables defining the system and the flow: the width (W), depth (H), radius (R) and shape of the microchannel, the maximum speed of the flow (U_m) and the particle hydrodynamic size (a; defined as the diameter in case of spherical particles)[3,15]. While this is the source of the potential for particle separation, it also makes designing the systems difficult and creates the need for extremely fine tolerances both in the fabrication and control of the flow rate (Q) in the operation of the systems. Because of this, engineering systems that exploit inertial focusing for practical applications remains challenging for those in the field and inaccessible for those outside. With this paper, extending our initial work[16], we aim at contributing to the field by making inertial focusing more accessible.

We recently presented inertial focusing in High Aspect Ratio Curved (HARC) microchannels[16], a

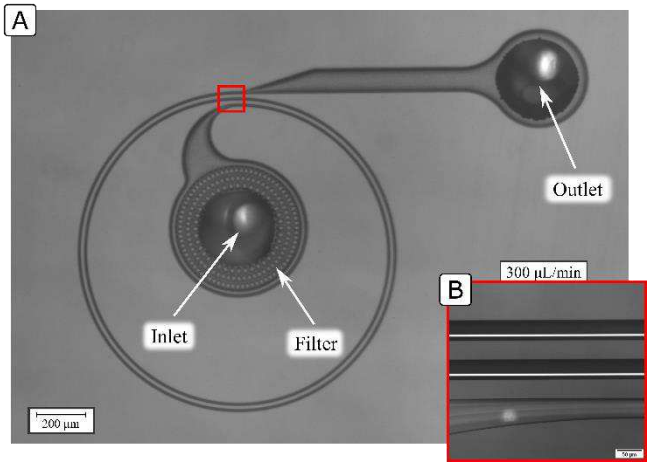

Figure 1. (A) Example of HARC system under the microscope. The red mark indicates the location where the high magnification pictures were taken for the evaluation of the performance of different devices (B) Example of performance with 4 µm polystyrene particles from a HARC system with two loops, 41x84 µm (WxH) and R 25 mm.

line of inertial focusing that is more intuitive than in other geometries and easily predictable. The systems consist of curved rectangular microchannels with $AR = H/W > 1$, in which the force field induced by the combination of F_L and F_D leads to all particles focusing into a single position that is stable within a wide range of flow rate. An example of HARC system built in silicon-glass is shown in Fig. 1A, and an example of focus performance in Fig. 1B.

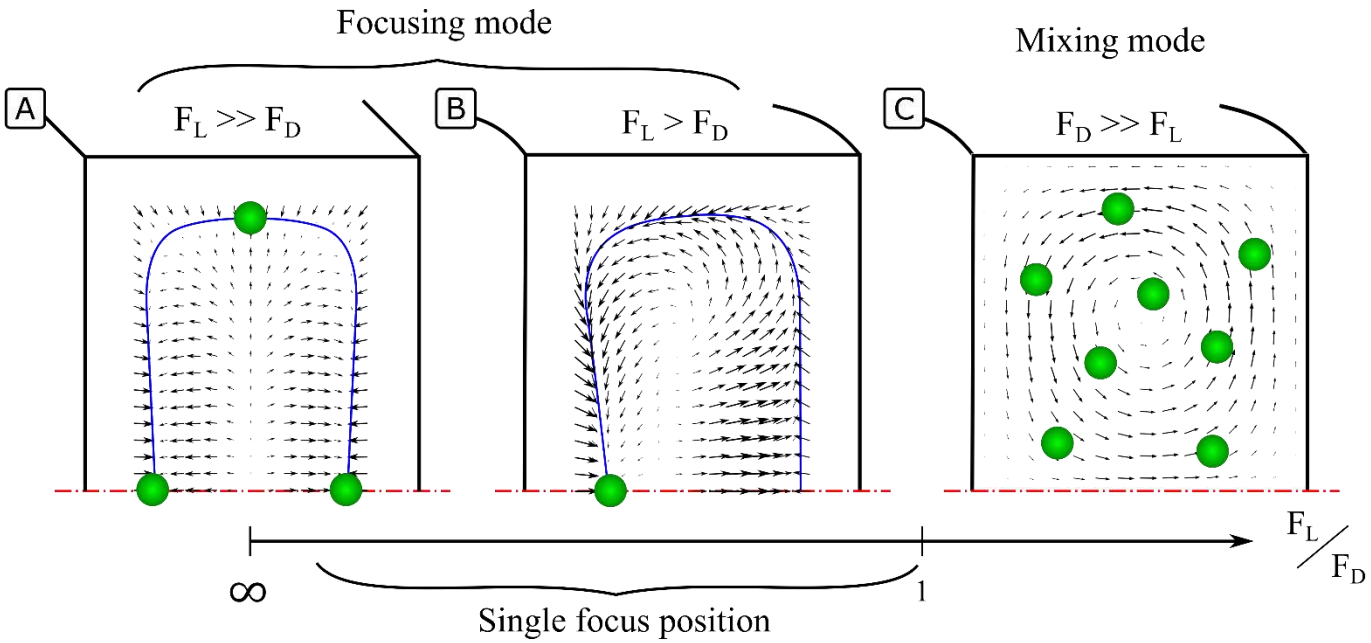

Figure 2. Force fields resulting from the combination of F_L and F_D in Inertial Focusing systems with high aspect ratio. The equilibrium perimeter (EP) is represented with a blue line. (A) Straight system. Only F_L is present, leading to four focus positions (B) Curved system where both forces are present and $F_L > F_D$. Particles focus into a single position. (C) Curved system where both forces are present and $F_D >> F_L$. Particles follow the vortexes indefinitely and remain unfocused.

Figure 2 shows different force fields in HARC microchannels depending on the ratio of the two forces.

The extreme case where the force field consists purely of F_L is similar to a straight microchannel, where a focus position is achieved at the centre of each wall, Fig. 2A. The other extreme, consisting purely of F_D, leads to particles following two symmetrical vortexes indefinitely, remaining randomly distributed, Fig. 2C. In an intermediate regime, however, where both forces are relevant but $F_L > F_D$ at the central region close to the inner wall, the resulting force field brings particles to a single equilibrium position, Fig. 2B.

To succeed in engineering a HARC system and achieve a single focus performance like that shown in Fig. 2B, two conditions must be met. First, all particles in the system should reach the focus position. Stemming from this condition, there is a lower limit of Q (Q_{min}) for the operation of the systems, for which an equation was proposed[16]. Second, F_L must be strong enough to stop the particles from crossing to the outer wall while following the secondary orbits. Stemming from this condition, HARC systems have an upper limit of Q (Q_{max}) over which F_D surpasses F_L and particles are not focused. This upper limit, the last piece to enable the complete design of HARC systems, remains unknown and is the focus of this work.

In this paper, we study the transition of HARC systems from focusing mode to mixing mode, i.e., the conditions where F_D surpasses F_L, with the aim of defining analytically the upper limit of the systems. We gathered experimental data of Q_{max} under different conditions from devices fabricated on silicon-glass and, together with a study about the strength of the secondary flow by COMSOL Multiphysics, we propose an equation that predicts the aforementioned upper limit. Last, the experimental measurements are linked to the strength of F_L, resulting in an experimental equation expressing its magnitude and scaling, which we believe may provide a valuable insight into the phenomenon of inertial focusing.

Theory of HARC Systems

In HAC systems, there is a net lift force (F_L) similar to that in straight channels, which makes particles migrate first to an equilibrium perimeter (EP) and slowly to the centre of the faces[17,18]; Fig 2A. The curvature of the system induces a secondary flow (perpendicular to the main flow) that takes the shape of two vortexes and drags particles in the direction of its streamlines[19]; Fig 2C. The novelty in HARC systems is that these secondary streamlines are mostly tangential to the EP and particles are easily swept over it until the central part of the inner wall [16]. In that region, the secondary flow turns and finds the opposition of F_L, whose horizontal component acts as a barrier (Lift Barrier; B_L). Provided that B_L is stronger than the drag by the secondary flow (F_D), particles are stopped and focused into a single position; Fig. 2B. If, on the contrary, B_L is not strong enough, particles go through and keep circulating indefinitely; Fig. 2C.

The study of inertial focusing in HARC microchannels can be divided in two sections: The collection of particles around the EP by the secondary flow, which was explained in detail in our previous work [16], and the retention/focus of particles at the inner wall; the focus of this paper.

Collection of particles around the cross section by the secondary flow

For particles to reach the single focus position, one Dean Loop must be completed (i.e., a full rotation of the secondary flow over the EP). The necessary channel length for this to happen, expressed as the number of loops (N_L):

$$N_L \approx \frac{20AR^2}{Re} \quad (1)$$

where Re is the Reynolds number of the channel, defined as $Re = \frac{\rho U_m W}{\mu}$, with ρ and μ being the density and dynamic viscosity of the fluid, respectively.

Rearranging Eq. 1, the minimum flow rate (Q_{min}) that will achieve focus for a given system with water-based samples is obtained:

$$Q_{min} \approx \frac{0.6AR^3W}{N_L}\frac{\mu L/min}{\mu m} \quad (2)$$

Retention/focus of particles at the inner wall

When particles reach the inner wall by following the secondary flow, the horizontal component of F_L acts as a barrier that hinders them from crossing to the outer wall (Lift Barrier; B_L). Provided that it is strong enough, the horizontal component of F_D (F_{Dx}) is cancelled and the vertical one brings all particles into a single focus position at the central part. If, on the contrary, F_{Dx} is stronger than B_L, particles continue following the secondary flow and remain unfocused.

Of particular interest is the fact that, for a given HARC system, increasing Q makes particles eventually surpass B_L, defining an upper limit of flow rate (Q_{max}) in the operation. This is not surprising, as F_D has been reported in multiple instances to grow faster with U than F_L[5,14,16,20–22]. At this particular event, F_{Dx} transitions from being weaker to being stronger than B_L. In other words, at that moment, both forces can be assumed to be equal; $F_{Dx} = B_L$, and, therefore, understanding F_D at these events leads to understanding B_L.

Figure 3 illustrates the performance of a HARC system before and after Q_{max}; Fig. 3A-B show the view under the microscope and Fig. 3C the intensity profile. It can be seen how a good quality focus is achieved at 540 µL/min ($Q < Q_{\max}$), while at 600 µL/min ($Q > Q_{\max}$) the system does not have the capacity to focus the particles any longer.

Rather than studying the force balance in the whole B_L, the analysis can be localized at the position where particles first breach the barrier. We identified such position to be at a distance approximately $W/3$ from the inner wall, the last position where particles focused experimentally prior to defocusing with further increase of Q, see Fig. 3. In the model used in this paper, further analysis of the phenomenon was done at this particular location. Figure 4A sketches the distribution of F_L proposed by Liu[22], isolating its horizontal value at $W/3$ from the inner wall (B_L). Figure 4B sketches the distribution of F_D in HARC

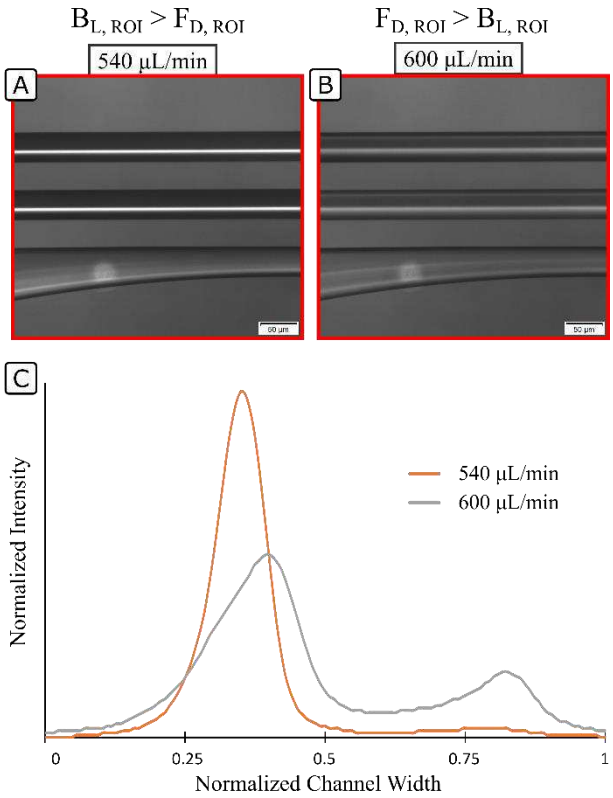

Figure 3. Example of performance with 4 µm polystyrene particles from a HARC system with two loops, 41x84 µm (WxH) and R 25 mm. The system focuses the particles at 540 µL/min, while they remain unfocused at 600 µL/min (A) View under the microscope. (B) Intensity profile.

channels obtained by COMSOL simulations, isolating its horizontal value at $W/3$ from the inner wall (F_{Dx}). Last, Fig. 4C shows the result of the combination of the two, where it can be seen how a further relative increase in F_D will first induce a breach in B_L right at the symmetry line.

The critical position, to which we refer as region of interest (ROI), is then defined at the symmetry line and $W/3$ from the inner wall, and the condition for HARC systems to focus particles:

$$B_{L,ROI} > F_{D,ROI} \quad (3)$$

Expressions for both $B_{L,ROI}$ and $F_{D,ROI}$ are derived in this paper.

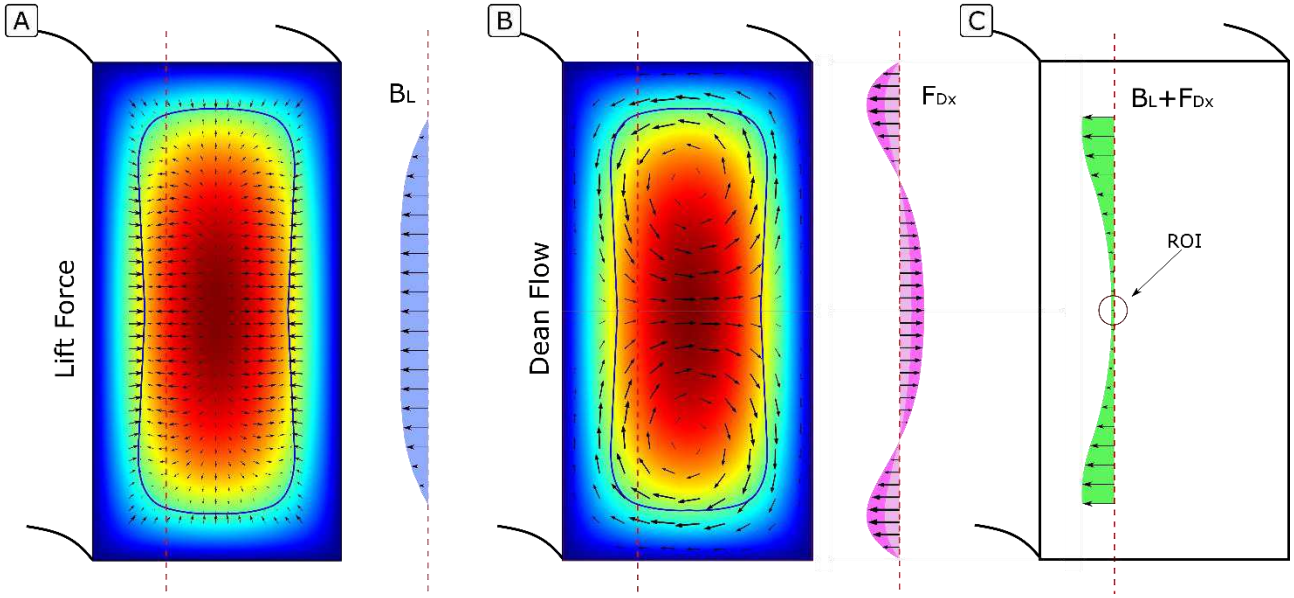

Figure 4. (A) Force field of F_L and isolation of the horizontal component at $W/3$ (B) Force field of F_D and isolation of the horizontal component at $W/3$. The different tonality of the isolated component indicates how it grows as the secondary flow gains strength. (C) Combination of both forces at $W/3$.

Material and Methods

Experimental evaluation of Q_{max}

The conditions that lead to F_D surpassing B_L were explored experimentally. We fabricated a set of devices with the same cross section (41x84 µm (WxH, measured values)), each consisting of one inlet, two loops with similar R and one outlet. The only variable that changed between devices was R, which ranged from 40 mm to 2.5 mm in a geometrical proportion of $\sqrt[4]{2}$, making a total of 17 devices. The microchannels were dry etched on silicon to avoid a possible deformation with the flow, sealed with glass and glass capillaries were used as fluidic connections. Further details about the fabrication process can be found in our previous work[16].

We mapped Q_{max} on a plot with Q in the Y axis and R in the X axis. For that, we ramped up Q while observing the outlet and considered B_L to be breached when the intensity near the outer wall started to increase and was ~2.5% of that near the inner wall. Particle sizes 8, 6, 4.8, 4, 3.2 and 2.2 µm in diameter were used.

The results with this first set of devices reflected the influence of U_m, a and R. To include W, we fabricated another set of devices with a cross section four times smaller (10.5x22 µm (WxH, measured values)) and R ranging from 5 mm to 0.6 mm in a geometrical proportion of $\sqrt[3]{2}$, making a total of 10 devices. Q_{max} was mapped in a similar way for such systems, using particle sizes 2.2, 1.0, 0.92, 0.79 and 0.7 µm in diameter.

Setup

Fluorescent polystyrene particles (0.70, 0.79, 0.92 and 1.0 µm, Thermo Scientific™ Fluoro-Max) were suspended in deionized water (with 0.1% of Triton X to reduce agglomeration) in a concentration of ~0.001 vol%.

An HPLC pump (Waters, model 515) was used to control the flow rate with a read out of the pressure.

An inverted fluorescence microscope was used (Olympus IX73 with an Orca-Flash 4.0 LT digital CMOS camera) for the observation of the systems.

Simulations

Simulations of the flow for different cross sections were performed using COMSOL Multiphysics v.5.5. The 3D flow of water at room temperature was solved using Navier-Stokes in HARC microchannels extending a quarter of a loop. The secondary flow was

analysed at a cross section ~2/3 of the channel length from the inlet to ensure a fully developed flow. The maximum size of the mesh elements was set to $W/30$ and the mesh was generated automatically. With the results, an analytical expression for $F_{D,ROI}$ was developed.

Expression for B_L

The conditions obtained experimentally for Q_{max} represent the particular situation where $F_{D,ROI}$ surpasses $B_{L,ROI}$. Introducing them into the analytical expression for $F_{D,ROI}$ was used to derive an expression for $B_{L,ROI}$.

Definition of the upper limit in HARC systems

The obtained expressions for $F_{D,ROI}$ and $B_{L,ROI}$ were substituted in Eq. 3, thereby defining analytically the upper limit where HARC systems focus particles.

Results and Discussion

Characterization of $F_{D,ROI}$ with COMSOL Multiphysics

COMSOL Multiphysics was used to simulate the flow in HARC microchannels with different cross sections; Fig. 5A. The magnitude of the secondary flow (U_D) at each point of the cross section scaled as $U_D = C\frac{\rho}{\mu}U_m^2W^2/R$, where C is a coefficient that depends on AR and adjusts the value to local positions. Values of C at the ROI (C_{ROI}) as a function of AR can be seen in Fig. 5B. An equation was fitted for $C_{ROI} = f(AR)$, obtaining an expression for the velocity of the secondary flow at the ROI ($U_{D,ROI}$):

$$U_{D,ROI} \approx C_{ROI}\frac{\rho}{\mu}\frac{U_m^2W^2}{R} \quad (4)$$

with $C_{ROI} = (6.55 - 1.87AR)\ 10^{-3}$ being accurate at least for AR between 1.5 and 3, which is the practical range of interest.

The drag force exerted by the secondary flow was calculated as a Stokes drag $F_D = 3\pi\mu a U_D^*$; where U_D^* is the relative speed of the particle compared to speed of the secondary flow. In the scenario where particles are focused, the relative speed is maximum; $U_D^* = U_{D,ROI}$, and $F_{D,ROI}$ becomes:

$$F_{D,ROI} = 3\pi a\ C_{ROI}\ \rho\frac{U_m^2W^2}{R} \quad (5)$$

With Eq. 5, the left side of Eq. 3 is defined, leaving the study of B_L to complete the equation.

Characterization of Q_{max}

Figure 6A shows the experimental results obtained for Q_{max} with the first set of devices (two loops, fixed R, 41x84 µm (WxH)). Each device allowed for the exploration of a vertical line on the graph; the flow rate was ramped up and the conditions where particles stopped being focused were marked. The transition was sharp for $Q > Q_{min} \approx 100$ µL/min for

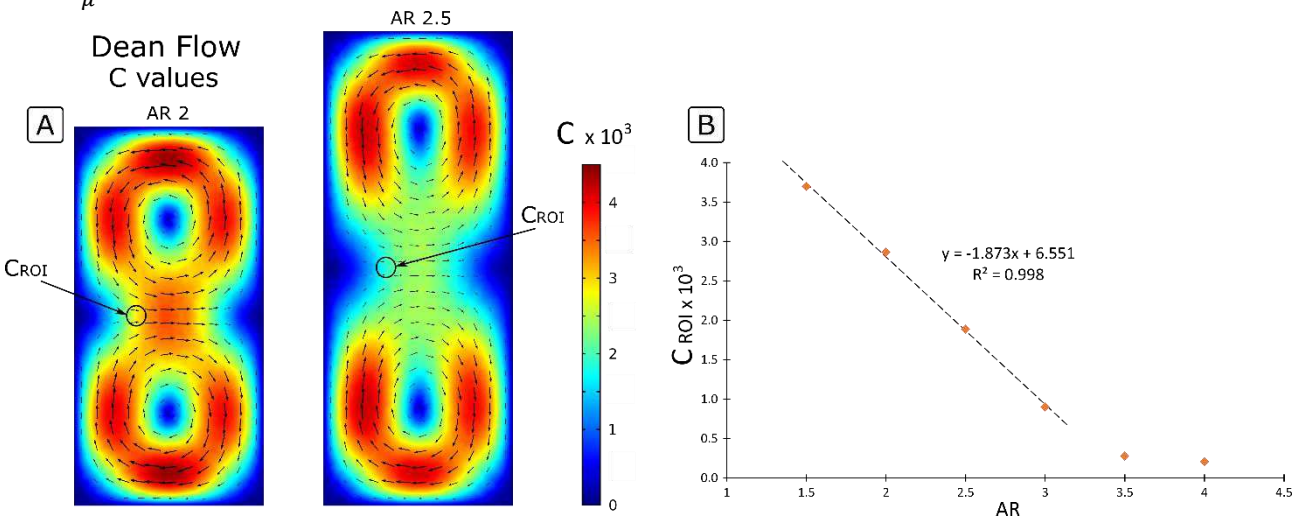

Figure 5. (A) Secondary flow in HARC systems with AR 2 and 2.5 and C value. (B) C value at the *region of interest* (ROI).

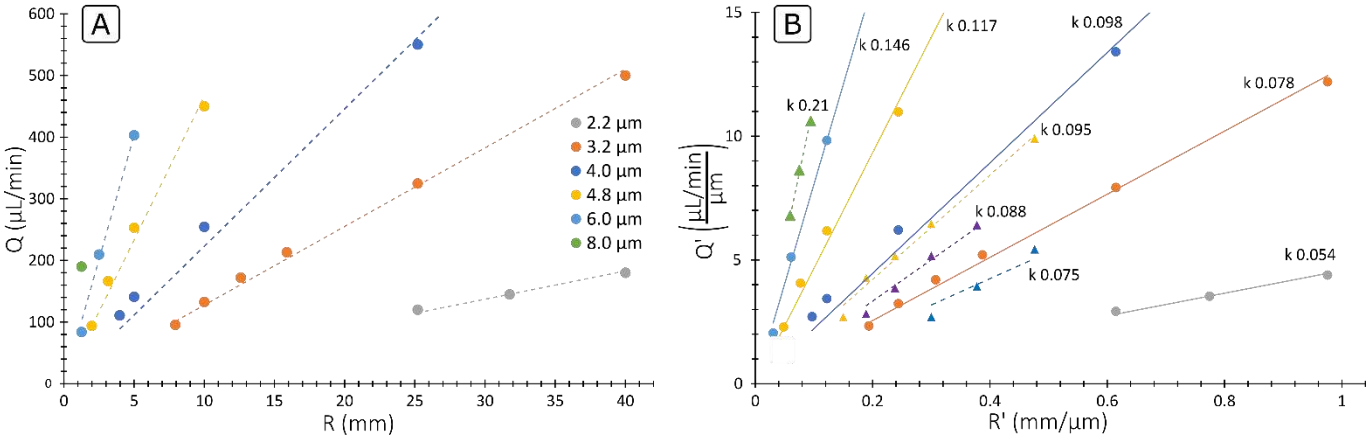

Figure 6. (A) Experimental data of Q_{max} obtained with microchannels consisting of two loops, fixed R and 41x84 µm (WxH). (B) Experimental data of Q_{max} expressed with generalized variables, $Q' = Q/W$, $R' = R/W$ and $k = a/W$. The data marked with circles corresponds to the set with cross section 41x84 µm (WxH) and the data marked with triangles to the set with cross section 10.5x22 µm (WxH).

said cross section and number of loops. For a given Q, smaller particles needed much larger R (weaker F_D) to remain focused, stemming from the known fact that F_L is weaker for smaller particles. For the same reason, for a given R, larger particles remained focused up to higher Q.

The plot was generalized by dividing the variables by W; obtaining $Q' = Q/W$, $R' = R/W$ and $k = a/W$. Figure 6B shows the data from both sets of devices together (41x84 µm and 10.5x22 µm) in such plot. Despite the scaling factor of four between them, all data fitted well and showed the same trend; see how the different lines obtained for all k values are well ordered and follow a linear trend.

The data from the first set was used to find the underlying pattern between Q' and R'. In Fig. 7, lines following the equation:

$$Q'_{max} = 27\, k^3 R' \frac{\mu L/min}{\mu m} \qquad (6)$$

are plotted together with the experimental data. It can be seen that the agreement is remarkable given the simplicity of equation. Note that, although both sets show the same trend, only the first one was used to find a fit because the relative errors in the small devices are expected to be larger, which is intrinsic to the technologies used for the fabrication; the possible lithography errors (hundreds of nm) and the roughness of the sidewalls by dry etching are the same in both cases, but the impact is much bigger for a small system.

Equation 6 can therefore be used to predict the line of Q_{max} with good accuracy for HARC systems with AR 2.05.

Finally, as it will be explained in the next sections, Eq. 6 can be extended for any AR with help of Eq. 4, obtaining:

$$Q_{max} = L\, k^3 R \qquad (7)$$

where $L = \frac{72AR}{C_{ROI} K_U} \frac{\mu L/min}{mm}$ and $K_U = (2.26 - 0.13AR)$.

With Eq. 7 defining the upper limit Q_{max}, together with Eq. 2 defining the lower limit Q_{min}, every piece to engineer HARC systems for particle focusing was obtained. Bringing them together, a range of flow rate where a HARC system focuses particles is defined:

$$\frac{0.6AR^3W}{N_L} < Q < L\, k^3 R \qquad (8)$$

Note that Eq. 6 was obtained from experimental data that covered the range Re 30 to 240 (with Re calculated using U_{max}). The approximation may be part of a more complex trend for lower and higher Re values.

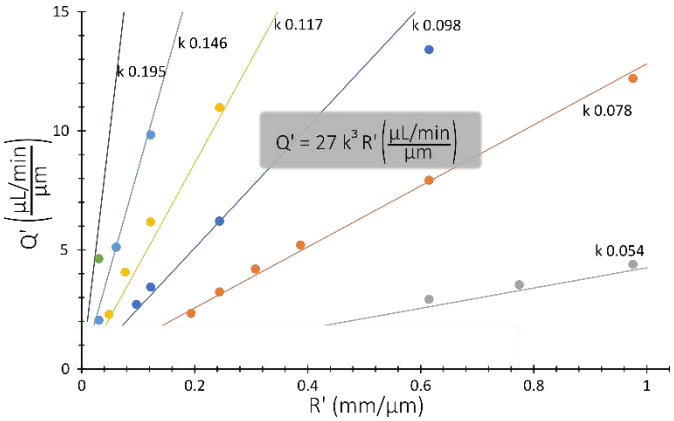

Figure 7. Analytical expression for Q'_{max} (Eq. 6, straight lines) together with experimental data from the first set (41x84 µm (WxH)).

Study of the Lift Barrier and relation with the lift force

From a practical point of view, Eq. 6 expresses the upper limit of Q over which particles breach the Lift Barrier of a microchannel with AR 2.05. But further than that, the equation contains the information of the particular event where $F_{D,ROI}$ surpasses $B_{L,ROI}$. Given that the expression for $F_{D,ROI}$ is known (Eq. 5), it can be used to derive an expression for $B_{L,ROI}$.

Equation 6 can be re-arranged so that $F_{D,ROI,AR\ 2.05}$ (Eq. 5 for AR 2.05) appears on the left side:

$$F_{D,ROI,AR\ 2.05} < J\ \rho\ \frac{U_m a^4}{W^3} \tag{9}$$

where $J = 3.6\ \pi\ 10^{-6}\ \frac{m^2}{s}$ is the Lift Barrier constant. See the ESI for a stepwise derivation.

By analogy with Eq. 3 ($F_{D,ROI} < B_{L,ROI}$), the right term of Eq. 9 is an analytical expression for $B_{L,ROI}$:

$$B_{L,ROI} = J\ \rho\ \frac{U_m a^4}{W^3} \tag{10}$$

Note that Eq. 10 is independent of AR. This fact was expected since B_L is born from the main flow and, at the symmetry line, this last is similar to a flow between two infinite parallel planes (Poiseuille flow, defined by U_m and W). In fact, assuming the dominant transversal force is F_L, $B_{L,ROI}$ coincides with the F_L induced on a particle in a Poiseuille flow at $W/3$ from the walls, being $F_L = f(U_m, W, a)$, as described by Ho and Leal in 1974[4]. Therefore, the expression for $B_{L,ROI}$ obtained experimentally in this paper can be considered as an expression for F_L at the ROI:

$$F_{L,ROI} = J\ \rho \frac{U_m a^4}{W^3} \tag{11}$$

with an experimentally measured scaling of F_L for Re between 30 and 240:

$$F_L \sim \rho \frac{U_m a^4}{W^3} \tag{12}$$

Interestingly, the scaling of the lift force here indirectly measured experimentally points at $F_L \sim U_m$, and agrees with other indirect measurements presented by Zhou et al., where the focus distance in straight channels with high aspect ratio was observed to be invariant with the flow rate up to moderate Re numbers[18] (Re 80 as reported by them, corresponding to Re 160 here, as they used the mean flow velocity for the definition, and here we use the maximum flow velocity). For higher Re, the focus length increased, which disagrees with our results. The discrepancy may originate in that the channels used to measure the focus length were fabricated on PDMS, which likely expands as the pressure is increased to reach higher Re, weakening F_L. In the present work, silicon microchannels were used, eliminating that possibility.

Generalization of the upper limit in HARC systems

Finally, introducing Eq. 5 and Eq. 10 into Eq. 3, the condition to be fulfilled for particles not to cross the Lift Barrier is generalized for any AR:

$$F_{D,ROI} < B_{L,ROI}$$

$$3\pi a\ C_{ROI}\ \rho \frac{U_m^2 W^2}{R} < J\ \rho\ \frac{U_m a^4}{W^3}$$

$$1 < \frac{J}{3\pi C_{ROI}} \frac{a^3 R}{U_m W^5} \tag{13}$$

Re-organizing Eq. 13 to have practical experimental variables:

$$Q < L\ k^3 R$$

$$Q_{max} = L k^3 R \tag{14}$$

where we coin $L = \frac{72AR}{C_{ROI}K_U}\frac{\mu L/min}{mm}$ as the HARC Limit coefficient. See ESI for a stepwise derivation.

With Eq. 14, we obtain the final expression for the upper limit of flow rate in HARC systems (Q_{max}) with AR between 1.5 and 3.

To summarize, in this paper we identified a critical position of the cross section of HARC microchannels where the balance of the lift force and the drag by the secondary flow defines if the system focuses the particles or not (*region of interest,* ROI). Analytical expressions for the calculation of the forces (Eq. 5 and 11) and their balance (Eq. 13) at said position are also provided. With this, the upper limit of flow rate of HARC systems is defined (Eq. 14) and, together with an expression for a lower limit (Eq. 1), it allows for an easy engineering of HARC systems for focusing particles. The experimentally measured strength of the lift force (Eq. 11) revealed a practical scaling law (Eq. 12), which we believe contributes to a better understanding of the phenomenon and may provide an interesting insight for the community.

Conclusions

With this work, the description of HARC systems for focusing particles is completed. The systems must be engineered to operate between two limits. The lower one was previously defined and ensures that particles have time to reach the focus position. The upper one, which is developed here based on experimental evidence, sets the limit where the lift force is no longer strong enough to stop particles from following the secondary flow and the system fails to focus them.

Expressions for the design of HARC systems that allow for a high quality, single position particle focusing are provided. Of special interest is the measured magnitude and scaling of the lift force, which may provide a valuable insight for the community.

We believe that HARC systems, with an intuitive focusing mechanism and two simple equations how to achieve a stable focus, make the technology of inertial focusing and its excellent performance easily accessible, which may facilitate its implementation outside research laboratories.

Data availability

Detailed mathematical derivations available in the Supplementary Information.

Competing interests

The authors declare no competing interests.

Notes and references

1. Martel, J. M. & Toner, M. Inertial Focusing in Microfluidics. *Annu. Rev. Biomed. Eng.* **16**, 371–396 (2014).
2. Zhang, J. *et al.* Fundamentals and applications of inertial microfluidics: A review. *Lab Chip* **16**, 10–34 (2016).
3. Chung, A. J. A Minireview on Inertial Microfluidics Fundamentals: Inertial Particle Focusing and Secondary Flow. *Biochip J.* **13**, 53–63 (2019).
4. Ho, B. P. & Leal, L. G. Inertial migration of rigid spheres in two-dimensional unidirectional flows. *J. Fluid Mech.* **65**, 365 (1974).
5. Asmolov, E. S. The inertial lift on a spherical particle in a plane poiseuille flow at large channel Reynolds number. *J. Fluid Mech.* **381**, 63–87 (1999).
6. Matas, J. P., Morris, J. F. & Guazzelli, E. Lateral Forces on a Sphere. *Oil Gas Sci. Technol. IFP* **59**, 59–70 (2004).
7. Di Carlo, D., Edd, J. F., Humphry, K. J., Stone, H. A. & Toner, M. Particle segregation and dynamics in confined flows. *Phys. Rev. Lett.* **102**, (2009).
8. Liu, C., Xue, C., Sun, J. & Hu, G. A generalized formula for inertial lift on a sphere in microchannels. *Lab Chip* **16**, 884–892 (2016).
9. Hood, K., Lee, S. & Roper, M. Inertial migration of a rigid sphere in three-dimensional Poiseuille flow. *J. Fluid Mech.* **765**, 452–479 (2015).
10. Segré, G. & Silberberg, A. Radial particle displacements in poiseuille flow of suspensions. *Nature* **189**, 209–210 (1961).
11. Warkiani, M. E. brahim. *et al.* Ultra-fast, label-free isolation of circulating tumor cells from blood using spiral microfluidics. *Nat. Protoc.* **11**, 134–148 (2016).
12. Zhou, J. *et al.* Isolation of circulating tumor cells in non-small-cell-lung-cancer patients using a multi-flow microfluidic channel. *Microsystems Nanoeng.* **5**, 8 (2019).
13. Cruz, J. *et al.* High pressure inertial focusing for separating and concentrating bacteria at high throughput. *J. Micromechanics Microengineering* **27**, 084001 (2017).
14. Cruz, J., Graells, T., Walldén, M. & Hjort, K. Inertial focusing

with sub-micron resolution for separation of bacteria. *Lab Chip* **19**, 1257–1266 (2019).
15. Martel, J. M. & Toner, M. Particle focusing in curved microfluidic channels. *Sci. Rep.* **3**, 1–8 (2013).
16. Cruz, J., Hjort, K. & Hjort, K. Stable 3D inertial focusing by high aspect ratio curved microfluidics. *J. Micromech. Microeng.* **31**, 015008 (2021).
17. Chun, B. & Ladd, A. J. C. Inertial migration of neutrally buoyant particles in a square duct: An investigation of multiple equilibrium positions. *Phys. Fluids* **18**, 031704 (2006).
18. Zhou, J. & Papautsky, I. Fundamentals of inertial focusing in microchannels. *Lab Chip* **13**, 1121–1132 (2013).
19. Squires, T. M. & Quake, S. R. Microfluidics: Fluid physics at the nanoliter scale. *Rev. Mod. Phys.* **77**, 977–1026 (2005).
20. Schonberg, J. A. & Hinch, E. J. Inertial migration of a sphere in Poiseuille flow. *J. Fluid Mech.* **203**, 517–524 (1989).
21. Matas, J. P., Morris, J. F. & Guazzelli, É. Inertial migration of rigid spherical particles in Poiseuille flow. *J. Fluid Mech.* **515**, 171–195 (2004).
22. Liu, C., Hu, G., Jiang, X. & Sun, J. Inertial focusing of spherical particles in rectangular microchannels over a wide range of Reynolds numbers. *Lab Chip* **15**, 1168–1177 (2015).

Figures

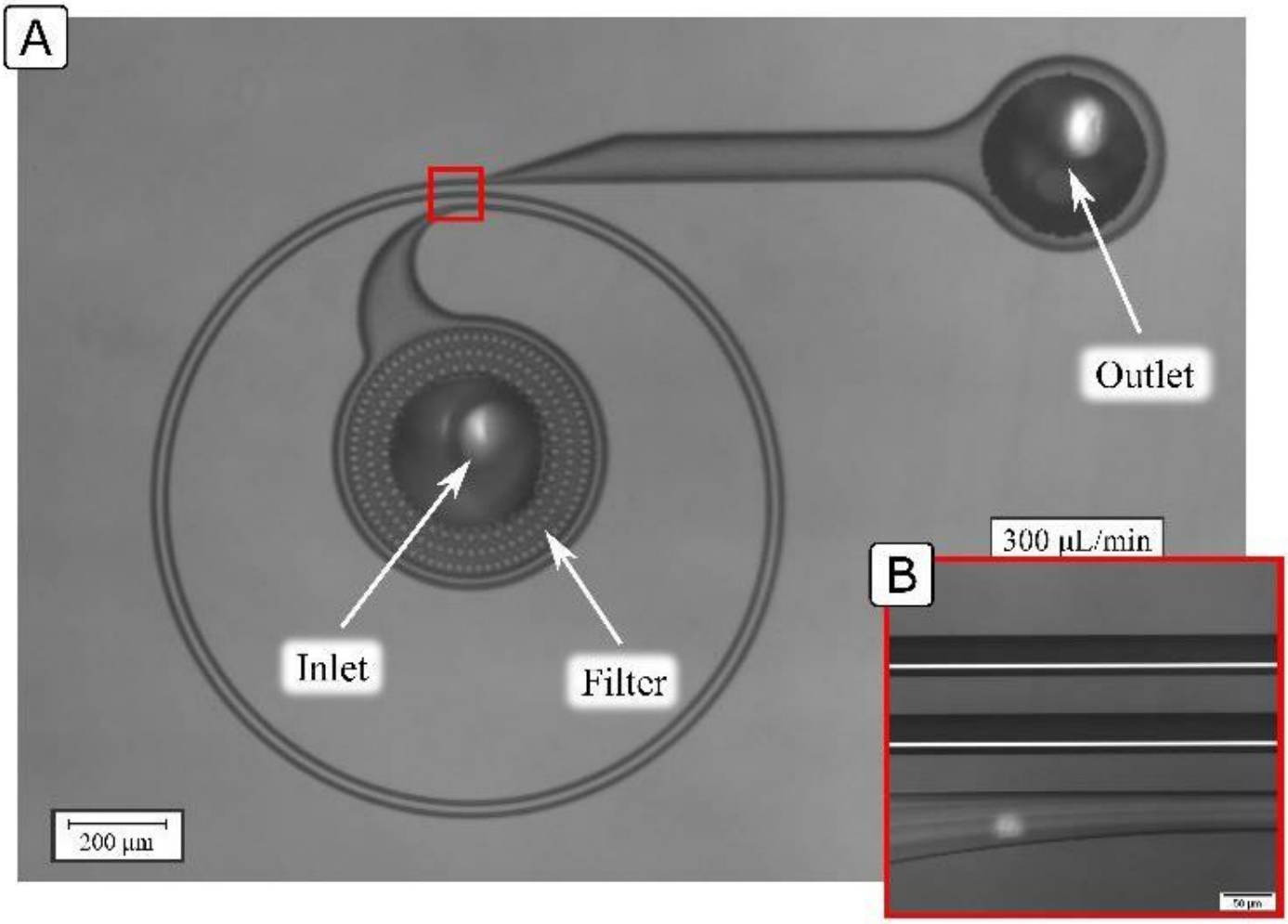

Figure 1

(A) Example of HARC system under the microscope. The red mark indicates the location where the high magnification pictures were taken for the evaluation of the performance of different devices (B) Example of performance with 4 µm polystyrene particles from a HARC system with two loops, 41x84 µm (□□□) and □ 25 mm.

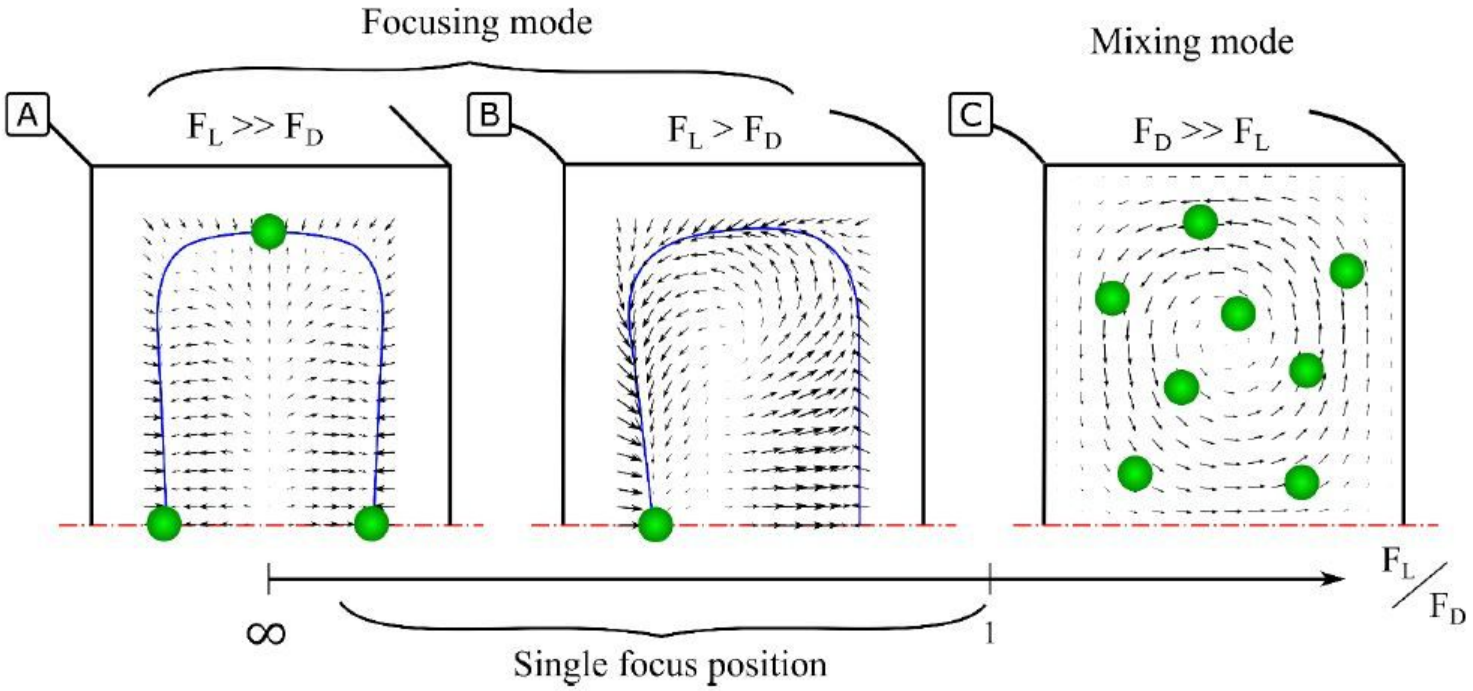

Figure 2

Force fields resulting from the combination of □□ and □□ in Inertial Focusing systems with high aspect ratio. The e quilibrium perimeter (EP) is represented with a blue line . (A) Straight system. Only □□ is present, leading to four focus positions (B) Curved system where both forces are present and □□>□□. Particles focus into a single position. (C) Curved system where both forces are present and □□>>□□. Particles follow the vortexes indefinitely and remain unfocused

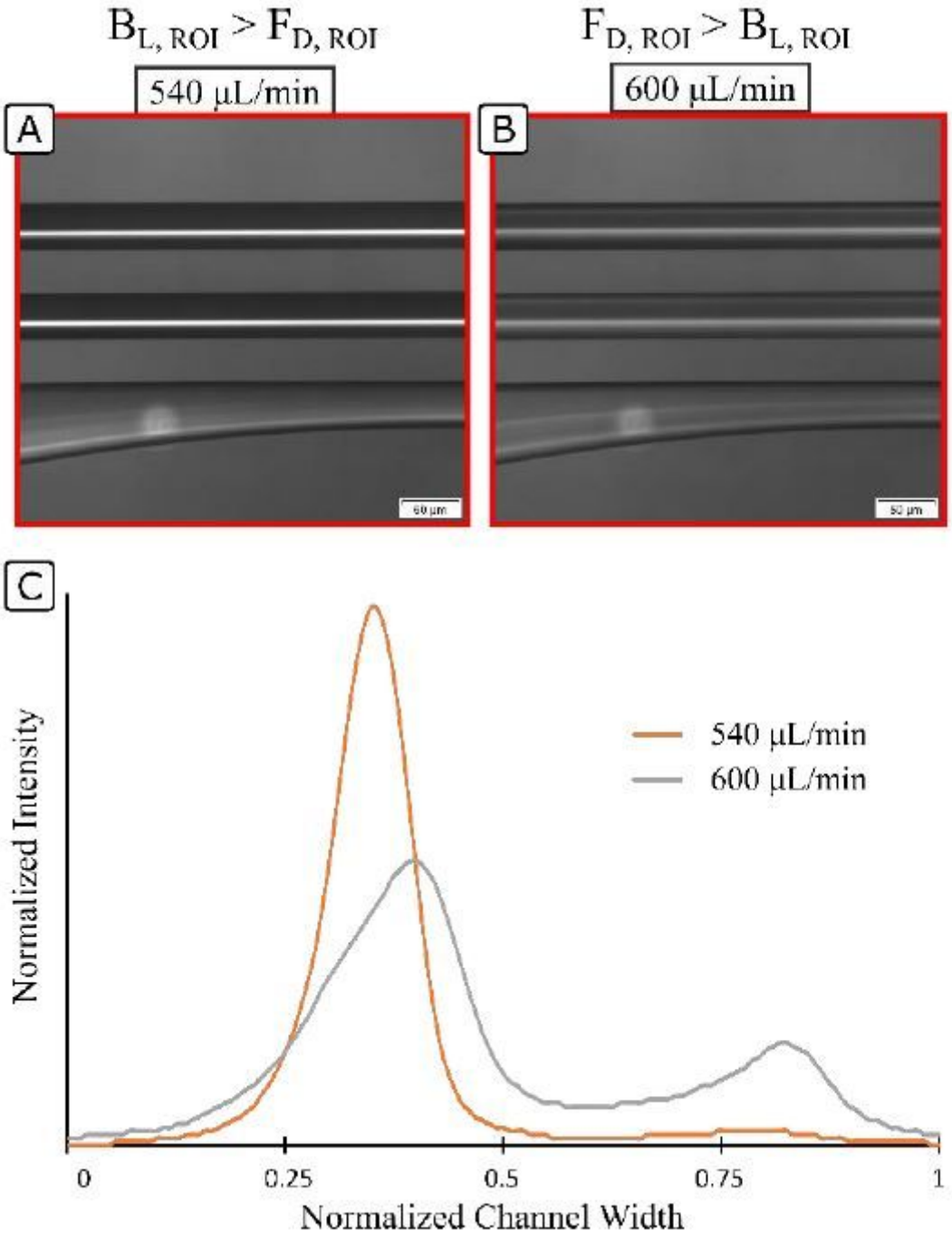

Figure 3

Example of performance with 4 µm polystyrene particles from a HARC system with two loops, 41x84 µm (□□□) and □ 25 mm. The system focuses the particles at 540 µL/min, while they remain unfocused at 600 µL/min (A) View under the microscope. (B) Intensity profile.

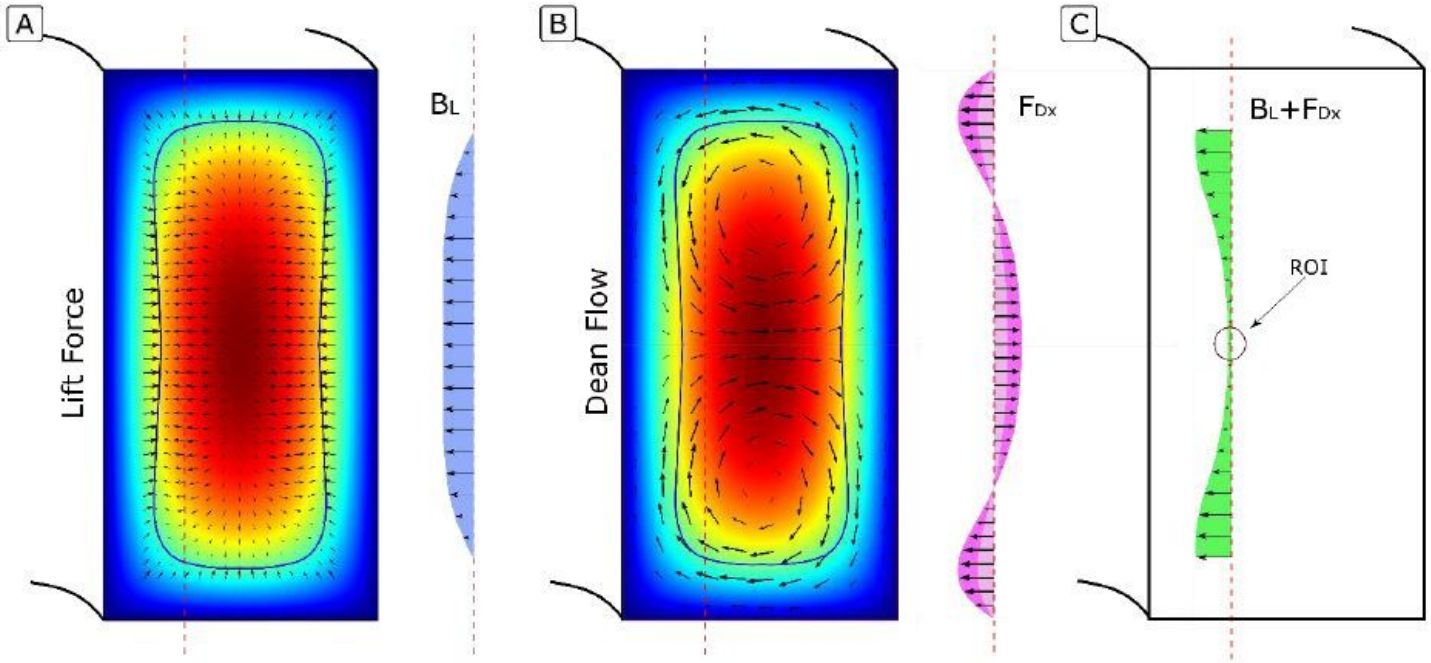

Figure 4

(A) Force field of ⁢⁢ and isolation of the horizontal component at ⁢/3 (B) Force field of ⁢⁢ and isolation of the horizontal component at ⁢/3. The different tonality of the isolated component indicates how it grows as the secondary flow gains strength. (C) Combination of both forces at ⁢/3

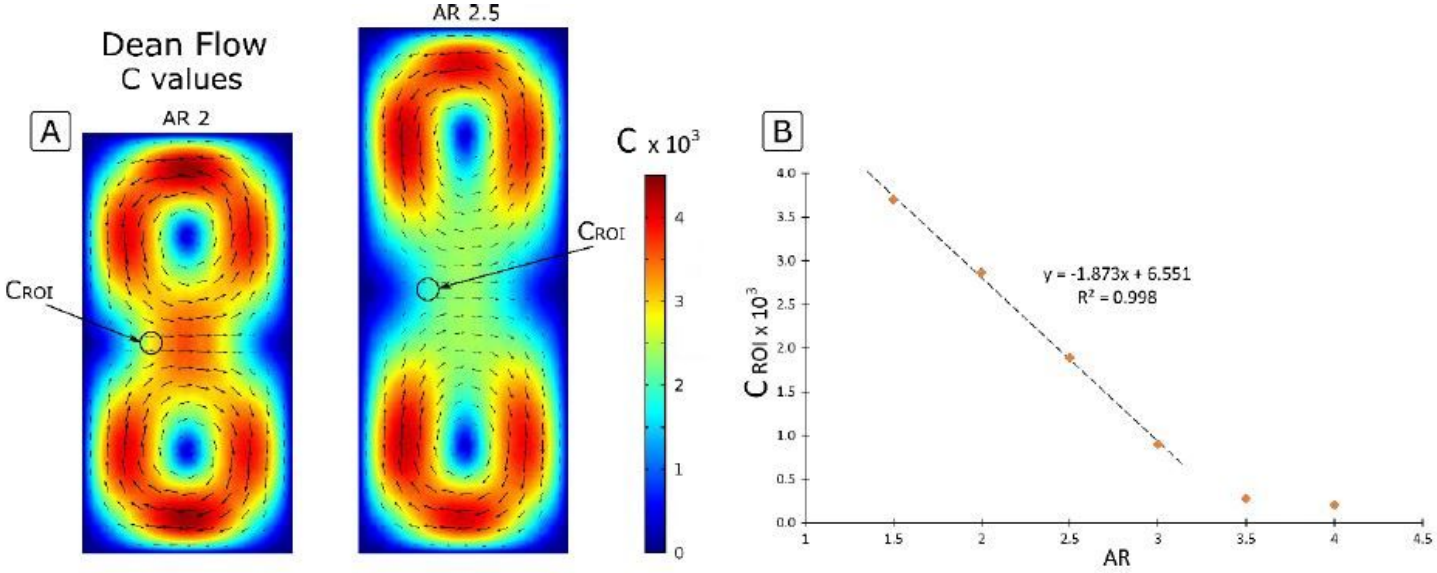

Figure 5

(A) Secondary flow in HARC systems with ⁢⁢ 2 and 2.5 and C value. (B) C value at the region of interest (ROI).

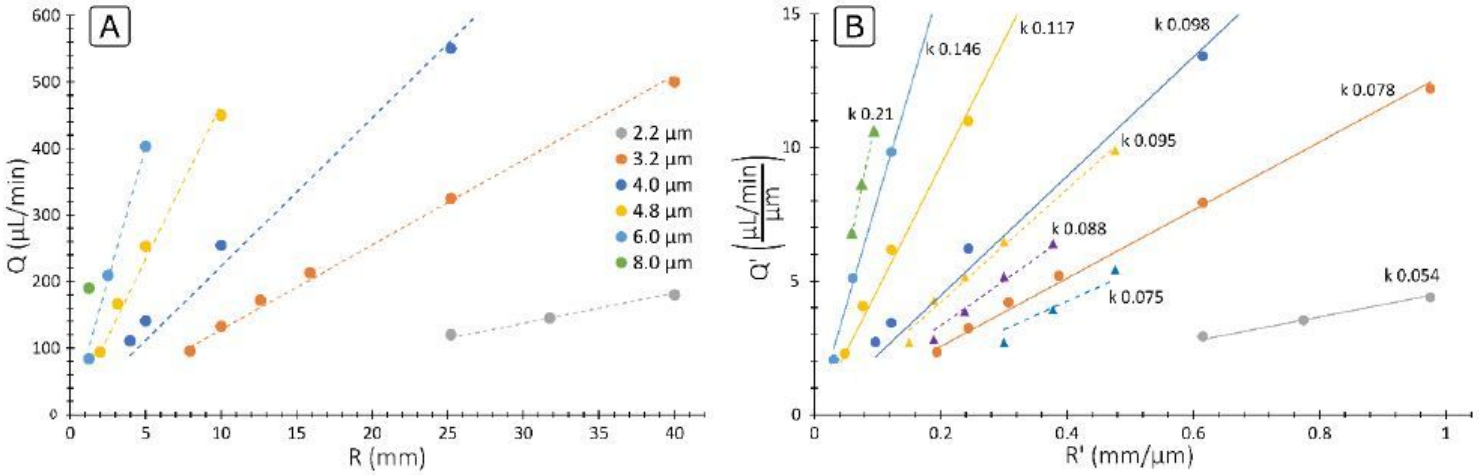

Figure 6

(A) Experimental data of □□□□ obtained w ith microchannels consisting of two loops, fixed □ and 41x84 µ m (□□□). (B) Experimental data of □□□□ expressed with generalized variables, □'=□□T⁄, □'=□□T and □=□□T⁄. The data marked with circles corresponds to the set with cross section 41x84 µm (□□□) and the data marked with triangles to the set with cross section 10.5x22 µm (□□□).

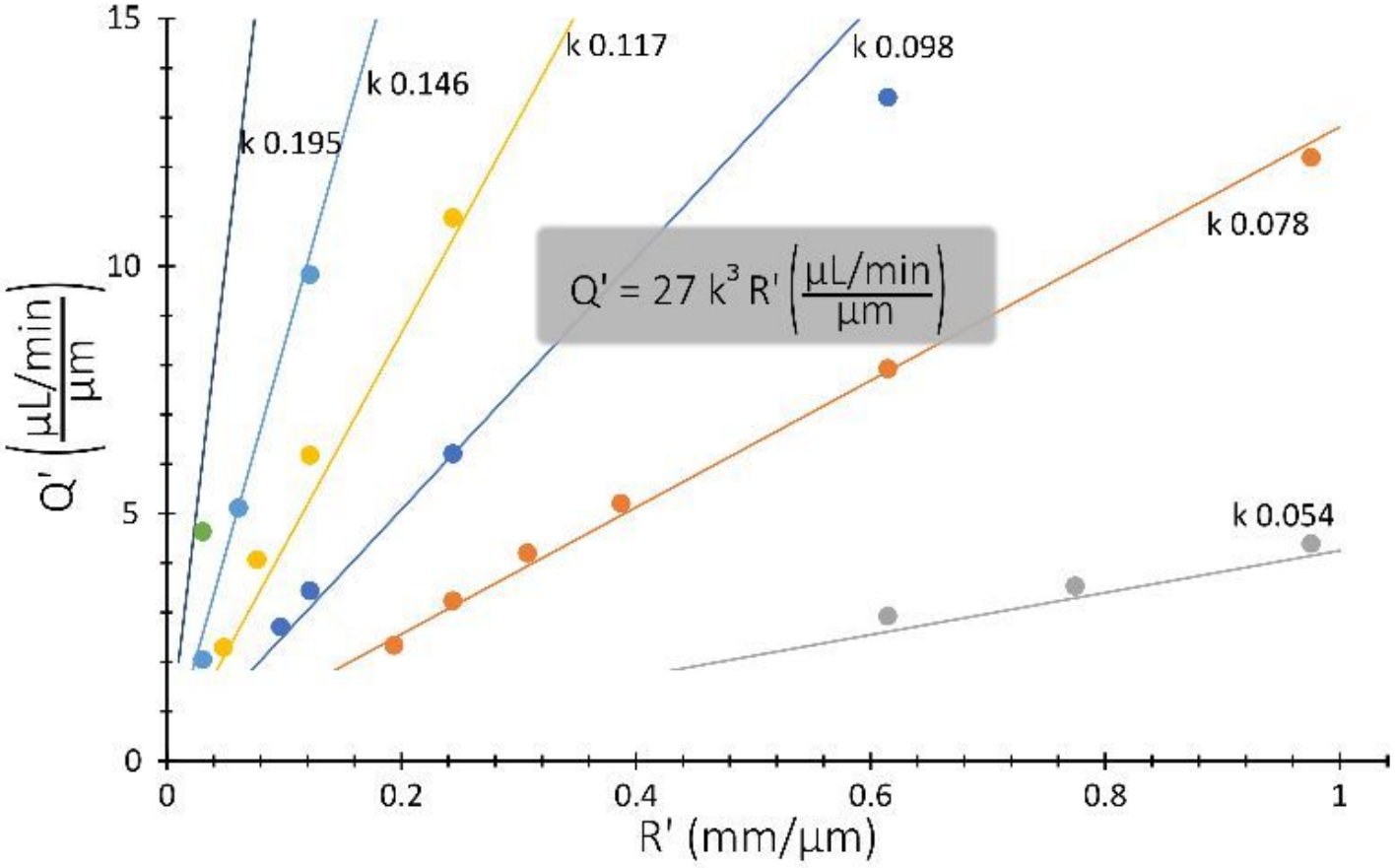

Figure 7

Analytical expression for □□□□' (Eq. 6, straight lines) together with experimental data from the first set (41x84 μm (□□□)).

Supplementary Files

This is a list of supplementary files associated with this preprint. Click to download.

- SupplementaryInformationFundamentalsofInertialFocusing.pdf